Validation of Parameterized Algorithms Used to Derive TRMM–CERES Surface Radiative Fluxes

SHASHI K. GUPTA

Analytical Services and Materials, Inc., Hampton, Virginia

DAVID P. KRATZ

Atmospheric Sciences, NASA Langley Research Center, Hampton, Virginia

ANNE C. WILBER

Analytical Services and Materials, Inc., Hampton, Virginia

L. CATHY NGUYEN

Science Applications International Corp., Hampton, Virginia

(Manuscript received 22 July 2003, in final form 30 December 2003)

ABSTRACT

Parameterized shortwave and longwave algorithms developed at the Langley Research Center have been used to derive surface radiative fluxes in the processing of the Clouds and the Earth's Radiant Energy System (CERES) data obtained from flight aboard the *Tropical Rainfall Measuring Mission* (*TRMM*) satellite. Retrieved fluxes were validated on an instantaneous–footprint basis using coincident surface measurements obtained from the Atmospheric Radiation Measurement (ARM) program's Southern Great Plains (SGP) central facility, the ARM/SGP network of extended facilities, and a number of surface sites of the Baseline Surface Radiation Network (BSRN) and the Climate Monitoring and Diagnostics Laboratory (CMDL). Validation was carried out separately for clear-sky and all-sky conditions. For the shortwave, systematic errors varied from -12 to 10 W m^{-2} for clear skies and from -5 to 35 W m^{-2} for all-sky conditions. Random errors varied from 20 to 40 W m^{-2} for clear skies but were much larger (45–85 W m^{-2}) for all-sky conditions. For the longwave, systematic errors were comparatively small for both clear-sky and all-sky conditions (0 to -10 W m^{-2}) and random errors were within about 20 W m^{-2}. In general, comparisons with surface data from the ARM/SGP site (especially the central facility) showed the best agreement. Large systematic errors in shortwave comparisons for some sites were related to flaws in the surface measurements. Larger errors in longwave fluxes for some footprints were found to be related to the errors in cloud mask retrievals, mostly during the nighttime. Smaller longwave errors related to potential errors in the operational analysis products used in satellite retrievals were also found. Still, longwave fluxes obtained with the present algorithm nearly meet the accuracy requirements for climate research.

1. Introduction

The radiative fluxes at the earth's surface are major components of the surface energy budget, and are as important to the study of weather and climate phenomena as radiative fluxes at the top of the atmosphere (TOA). These fluxes play an important role in oceanic and atmospheric general circulation patterns (Ramanathan 1986; Wild et al. 1995). Developing a long time series of the surface radiation budget (SRB) is essential for accomplishing the objectives of a number of World Climate Research Program (WCRP) projects, such as the International Satellite Land Surface Climatology Project (ISLSCP) and the Global Energy and Water-cycle Experiment (GEWEX) (Suttles and Ohring 1986; Schmetz 1989). Presently, the WCRP/GEWEX Radiation Panel is sponsoring the development of long time series of SRB parameters at high spatial and temporal resolution under the National Aeronautics and Space Administration (NASA)–GEWEX SRB project (Stackhouse et al. 2002).

The Clouds and the Earth's Radiant Energy System (CERES) project is an investigation of cloud-radiation feedbacks in the earth's climate system (Wielicki et al. 1996). CERES spaceborne radiometers measure broadband shortwave (SW) and longwave (LW) radiances at

Corresponding author address: Dr. Shashi K. Gupta, Analytical Services and Materials, Inc., 1 Enterprise Pkwy., Ste. 300, Hampton, VA 23666.
E-mail: s.k.gupta@larc.nasa.gov

the TOA. The first in a series of CERES instruments was launched into a low-inclination (35°) orbit in November 1997 aboard the *Tropical Rainfall Measuring Mission* (*TRMM*) satellite. The CERES instrument on board *TRMM* successfully operated from January to August 1998 and during March 2000. Four more CERES instruments have subsequently been launched and are currently operating on board Earth Observing System (EOS) satellites: two each on *Terra* and *Aqua.*

Deriving reliable estimates of SRB parameters is also an important objective of the CERES project for developing a complete picture of the earth–atmosphere system. Since the SRB cannot be directly and uniquely measured by satellite-borne instruments, the surface fluxes are derived with several different methods using combinations of radiation models, data assimilation products, and satellite measurements. The Surface and Atmospheric Radiation Budget (SARB; Charlock et al. 1997) component of CERES represents one such method where SW and LW fluxes at the surface, at three levels in the atmosphere, and at the TOA are computed with a radiative transfer model.

In addition to SARB, surface fluxes are being derived within CERES using two SW and two LW models, which are based on TOA-to-surface transfer algorithms or fast radiation parameterizations. These models are the Li et al. (1993) model (SW model A), the Darnell et al. (1992) model (SW model B), the Inamdar and Ramanathan (1997) model (LW model A), and the Gupta et al. (1992) model (LW model B). These four models were incorporated into CERES processing to provide independent sources of surface fluxes to compare with SARB results, and in recognition of the fact that all model results are subject to uncertainties. All of these models are very fast in comparison to SARB and thus allow for earlier testing of time-averaged and interpolated results while making minimal demands on computer resources. The SW and LW models B, having been developed at NASA Langley Research Center (LaRC) are presently called the Langley Parameterized Shortwave Algorithm (LPSA) and the Langley Parameterized Longwave Algorithm (LPLA), respectively. Both LPSA and LPLA are also being used in the NASA–GEWEX SRB project where long time series of SRB parameters are being developed on a $1° \times 1°$ global grid and at 3-hourly temporal resolution. The GEWEX SRB project makes use of satellite-derived cloud properties and reanalysis meteorological data with LPSA–LPLA and two other radiative transfer based algorithms to compute the SRB fields (Stackhouse et al. 2002). The LPSA–LPLA algorithms thus constitute a valuable linkage between CERES and GEWEX SRB projects with possibilities of cross validation.

This paper presents validation of the instantaneous surface fluxes derived on a CERES scanner footprint basis with the Langley algorithms (the B models) for both clear-sky and all-sky conditions. Fluxes from these models were derived and archived as part of the single-scanner footprint (SSF) product of CERES processing. The present study is limited to the validation of fluxes for the January–August 1998 period from the CERES instrument on board the *TRMM* satellite. A brief description of the B models is presented in section 2. The sources and main characteristics of the validation datasets are described in section 3. Validation of all satellite-derived fluxes and resulting error statistics are presented in section 4, while section 5 presents the summary and conclusions.

2. The models

a. SW model

The SW model (LPSA; Gupta et al. 2001) consists of physical parameterizations that account for the attenuation of solar radiation in simple terms separately for a clear atmosphere and for clouds. Surface insolation, $F_{\rm sd}$, is computed as

$$F_{\rm sd} = F_{\rm toa} T_a T_c, \tag{1}$$

where $F_{\rm toa}$ is the corresponding TOA insolation, T_a is the transmittance of the clear atmosphere, and T_c is the transmittance of the clouds (Darnell et al. 1988; Darnell et al. 1992). Instantaneous values of $F_{\rm toa}$ were available in the CERES processing system and were computed with standard textbook procedures (e.g., Peixoto and Oort 1993). Clear-sky transmittance, T_a, was computed as

$$T_a = (1 + B) \exp(-\tau_z), \tag{2}$$

where B represents the backscattering of surface-reflected radiation by the atmosphere (gases and aerosols) and τ_z is the broadband extinction optical depth at solar zenith angle z, which accounts for absorption and backscattering in the clear atmosphere. Cloud transmittance, T_c, was computed using a threshold method (see Darnell et al. 1992) as

$$T_c = 0.05 + 0.95[(R_{\rm ovc} - R_{\rm meas})/(R_{\rm ovc} - R_{\rm clr})], \tag{3}$$

where $R_{\rm ovc}$, $R_{\rm clr}$, and $R_{\rm meas}$ represent values of overcast, clear, and measured reflectances for the footprint, respectively. Equation (3) is based on standard threshold methods used for cloud parameter determination (e.g., Möser and Raschke 1984) and recognition of the observational fact that even for the thickest clouds, T_c is not reduced to 0. The value of $R_{\rm ovc}$ for the footprints was computed from an empirical relation developed from International Satellite Cloud Climatology Project (ISCCP; Rossow and Schiffer 1991) data and $R_{\rm clr}$ was obtained from the monthly clear-sky reflectance climatologies developed from Earth Radiation Budget Experiment (ERBE; Barkstrom et al. 1989) data. For a detailed description of LPSA, the reader is referred to Gupta et al. (2001).

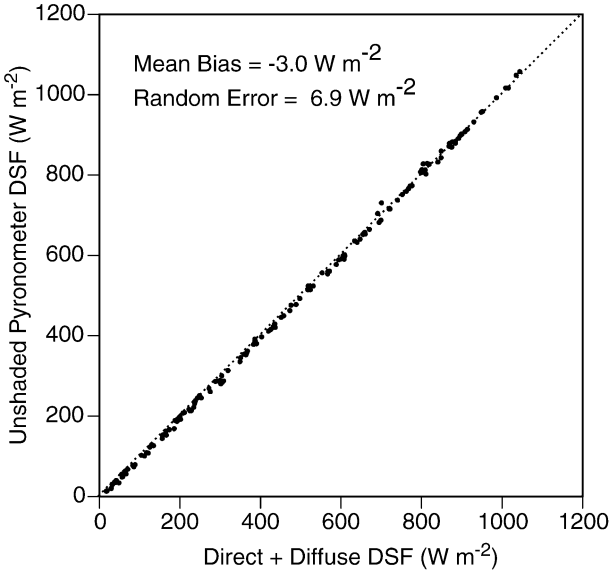

FIG. 1. Comparison of all-sky downward SW fluxes measured at the ARM/CF with unshaded pyranometer and the direct + diffuse method. These are the same 152 points for which the statistics of comparison between CERES-derived and unshaded pyranometer DSF are shown in the lower box in Table 1. Mean bias and random error for this comparison were -3.0 and 6.9 W m^{-2}, respectively. This and many similar comparisons showed the differences between the two methods to be small.

b. LW model

The LW model (LPLA; described in Gupta et al. 1992) is a fast parameterization developed from an accurate narrowband radiative transfer model (Gupta 1989) in which downward LW flux (DLF) is computed in terms of an ''effective emitting temperature'' of the atmosphere, the column water vapor, the fractional cloud amount, and the cloud-base height for each footprint. The effective emitting temperature is a weighted average of the surface skin temperature and temperatures of the lower-tropospheric layers. The effective emitting temperature and column water vapor are computed from the temperature and humidity profiles available from the Meteorology, Ozone, and Aerosol (MOA) Meteorological Database maintained for all CERES processing (Gupta et al. 1997). Presently, MOA profiles are based on operational analysis products obtained from the European Centre for Medium-Range Weather Forecasts (ECMWF). Fractional cloud amount and cloud-base height are available at the time of flux computation from the cloud subsystem of CERES processing (Minnis et al. 1997) where they are derived using high-resolution imager data from the Visible/Infrared Scanner (VIRS), which is also being flown aboard the *TRMM* satellite.

The SW and LW models described above have undergone extensive validation in the past, both against ground-based flux measurements and other more detailed radiative transfer model computations. Validation of the SW model was mostly done using ground-based measurements (Darnell et al. 1988; Darnell et al. 1992; Gupta et al. 1999). Longwave model validation was done against ground-based measurements (Gupta et al. 1999) and also against detailed models including line-by-line standards in the context of the Intercomparison of Radiation Codes in Climate Models (ICRCCM; Gupta et al. 1992, 1993; Ellingson et al. 1991).

3. Surface data for validation

High quality ground-based radiometric measurements needed for validating surface flux algorithms were not available until just a few years ago. Before the advent of high quality surface measurements, validation was attempted by comparing these algorithms with line-by-line and other detailed radiative transfer models available within the framework of ICRCCM-type projects (Ellingson et al. 1991). With the initiation of a number of measurement programs, there are now a number of networks that provide high quality radiometric measurements from sites around the globe. Several of these networks were operational in 1998 and, therefore, ground-based measurements were available for validation during the period of TRMM–CERES observations. Most important among these sites were the U.S. Department of Energy's Atmospheric Radiation Measurement (ARM; Stokes and Schwartz 1994) program's Southern Great Plains (SGP) facilities. These included the ARM central facility (ARM/CF) located near Lamont, Oklahoma, and a mesoscale network of about 20 extended facilities (ARM/EF) spread over central Oklahoma and southern Kansas. ARM datasets used in the present work were acquired with the Solar Infrared Radiation Station (SIRS) set of instruments at the SGP central and extended facilities. In addition, surface datasets were obtained from the Florianopolis, Brazil; Alice Springs, Australia; and Tateno, Japan, sites of the Baseline Surface Radiation Network (BSRN; Ohmura et al. 1998), and the Bermuda and Kwajalein (U.S. Marshall Islands) sites of the National Oceanic and Atmospheric Administration/Climate Monitoring and Diagnostics Laboratory (NOAA/CMDL) network. The authors obtained these datasets from the CERES/ARM Validation Experiment (CAVE; Rutan et al. 2001) database, which is maintained at NASA LaRC in a Web-accessible form for use in the CERES project and is available also to the outside science community. Because of the limited coverage due to the low inclination of the TRMM orbit, the selection of validation sites was restricted to the range of $\pm 38°$ latitude. One-minute averages of downward SW and LW fluxes were available from all of these sites with the exception of Florianopolis, for which the averaging interval was 2 min. Temporal matching of the satellite and site fluxes was done at the highest resolution of the site data, that is, 1 or 2 min. Spatial matching was done to a distance of 10 km between the location of the site and the center of the CERES footprint. Values for all CERES footprints

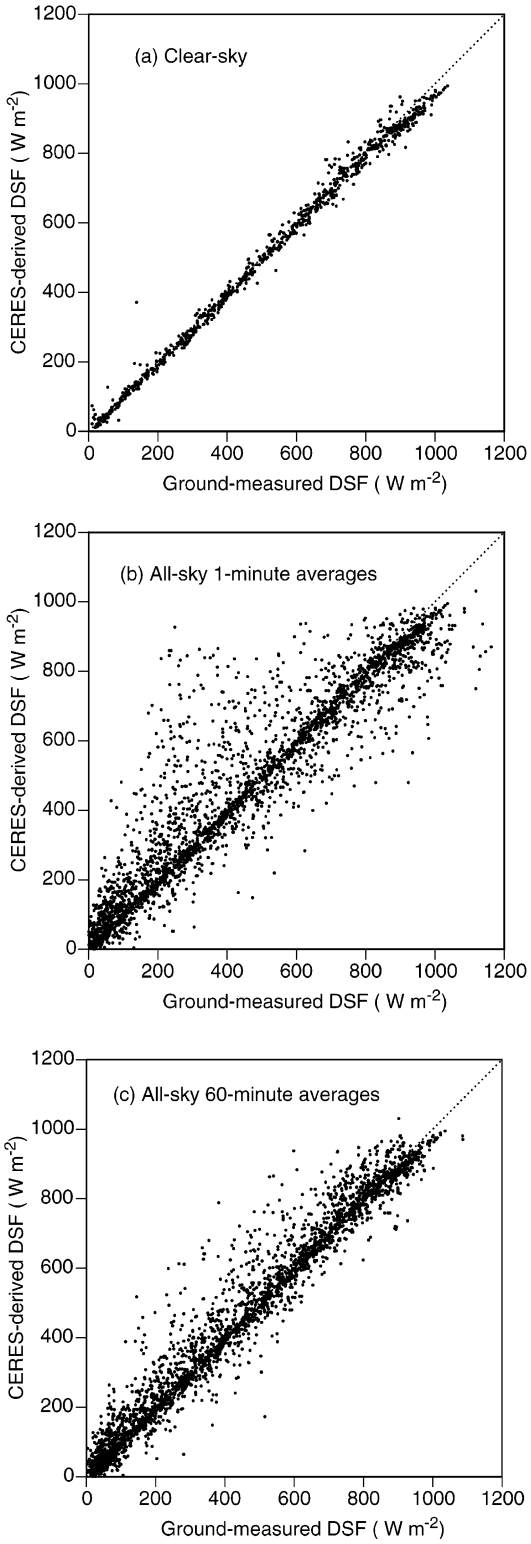

FIG. 2. Comparisons of DSFs derived from the CERES algorithm to ground-based measurements combined from all ARM/CF, ARM/EF, BSRN, and CMDL sites: (a) clear-sky conditions where ground-measured fluxes are 1-min averages, (b) all-sky conditions; ground-measured fluxes are 1-min averages, and (c) all-sky conditions where ground-measured fluxes are 60-min averages. Error statistics for (a) and (c) are presented in the upper and lower boxes of Table 1, respectively. Comparison of (b) to (c) shows a small change in the mean bias (from 14.1 to 12.8 W m^{-2}), but a significant reduction in the random error (from 99.6 to 61.4 W m^{-2}).

within the 10-km range of the sites and within the 1- (or 2) min interval were averaged together for comparison with the corresponding ground-based values.

At most of the above sites, surface insolation estimates were obtained concurrently by two methods. The first method uses an unshaded pyranometer to measure the hemispheric or global irradiance. The second method combines the direct horizontal fluxes derived from a normal incidence pyrheliometer (NIP) measurement with diffuse horizontal flux measured with a shaded pyranometer to constitute the total irradiance. The second method is considered more accurate (Michalsky et al. 1999), especially for clear conditions, because the unshaded pyranometer measurements are subject to cosine errors. Also, the calibration of unshaded pyranometers is based on measurements made for solar zenith angles in the 45°–55° range, which leads to an overestimation at low values of solar zenith angles and an underestimation at high values (Augustine et al. 2000). However, the advantage of the second method is highly dependent on the faultless functioning of two solar-tracking devices and, therefore, on a high level of monitoring and maintenance. We found large discrepancies and frequent data gaps in the insolation estimates from many sites obtained with the second method, most of which were traced back to malfunctions in the solar-tracking components of the instruments. By contrast, measurements obtained from the first method (unshaded pyranometers) had fewer data gaps and other discrepancies at most sites. In addition, the advantage of the second method is much smaller under cloudy conditions as illustrated by Fig. 1, which shows a scatterplot of all-sky insolation estimates obtained with the two methods during January–August 1998 at the ARM/CF site. We, therefore, decided to use the unshaded pyranometer measurements in these SW comparisons to maintain consistency across all sites and enable the use of as much ground data as possible. The downward LW fluxes were obtained at all sites using a single set of pyrgeometer measurements that exhibited no obvious problems.

4. Results and discussion

Figure 2a shows a scatterplot of CERES-derived and ground-measured clear-sky downward SW fluxes (DSFs) for all sites used in this study. Multiple sites were combined in each scatterplot in this section to limit the number of figures. The number of points and error statistics for clear-sky SW comparisons are presented in the upper box of Table 1 separately for each group of

TABLE 1. Error statistics for comparisons of CERES-derived and ground-measured surface SW fluxes. Fluxes in column 3 of this table and in Tables 2 and 3 are the mean values of CERES-derived fluxes.

Site(s)	No.	Flux (W m^{-2})	Bias (W m^{-2})	RE (W m^{-2})
Clear-sky SW flux statistics				
ARM/CF	54	519.4	−11.6	17.9
ARM/EF	764	522.5	−8.1	19.0
BSRN	52	461.2	−8.4	41.8
CMDL	26	744.7	10.6	39.1
All sites	896	525.2	−7.8	22.3
All-sky SW flux statistics				
ARM/CF	152	457.8	−5.3	46.1
ARM/EF	2141	476.0	10.7	56.4
BSRN	263	375.8	7.4	58.9
CMDL	371	427.3	35.9	85.4
All sites	2927	459.9	12.8	61.4

sites, namely, the ARM/CF, ARM/EF, BSRN, and CMDL, and for a combination of all groups. A similar scatterplot for all-sky SW fluxes for all sites is shown in Fig. 2b. The excessive scatter in Fig. 2b (99.6 W m^{-2}), over 4 times greater than the scatter in Fig. 2a, is indicative of the large spatial variability of clouds in the one or more CERES footprints that contribute to the 1-min averages around each ground site. The large spatial variability of clouds within the footprint created a situation where surface measurements over 1-min intervals were not representative of surface conditions over the entire footprint. An attempt to compensate for the effect of cloud spatial variability was made by averaging each 1-min ground measurement over longer intervals. Trials with 2-, 5-, 15-, 30-, and 60-min averaging showed significant decreases in random error up to 30 min and little change from 30 to 60 min. Averaging over longer than 60 min reduced the number of daytime points with no apparent benefit. The 60-min averaging interval ($\pm$30 min from the actual match time) was, therefore, adopted as the optimum. A comparison of the same matched fluxes after the 60-min averaging is presented in Fig. 2c and shows that, while the bias changes little, the random error is greatly reduced (61.4 W m^{-2}). The all-sky SW results presented in the lower box in Table 1 for each group separately, and for all sites together, are for comparisons with the 60-min averages. Error statistics in Table 1 show that the bias error varies widely among the sites for both clear-sky and all-sky conditions. Random error (RE) varies from 18 to 42 W m^{-2} for clear skies and from 46 to 85 W m^{-2} for all-sky conditions. The large values of random error for all-sky conditions seen here are comparable to those found in other studies, for example, by Rossow and Zhang (1995) and Gautier and Landsfeld (1997). These comparisons, and a few others not presented here, show that errors for ARM/SGP sites are lower than those for BSRN or CMDL sites. Problems encountered with surface data from BSRN and CMDL sites in the early stages of this investigation were brought to the attention of scientists from those organizations and were promptly corrected by them (E. Dutton 2003, personal communication). Only the corrected versions of BSRN and CMDL data were used in this investigation. Random errors for all-sky comparisons are higher than for clear-sky comparisons because satellite and ground instrument fields of view can be substantially different and spatial distribution of cloudiness in the two may also be quite different. Of course, ground-measured fluxes have their own errors and a part of the above errors may be coming from there. Global flux (direct + diffuse) measurements used here, especially those for clear-sky conditions, are subject to significant negative biases related to thermal offsets (Philipona 2002).

Corresponding scatterplots for clear-sky and all-sky LW fluxes combined for all sites are presented in Figs. 3a and 3b, respectively. Error statistics for each group separately and for all groups combined are presented in Table 2. For LW fluxes, both bias and random errors are comparable in magnitude between clear-sky and all-sky conditions. Biases for the ARM/SGP sites are significantly lower than for BSRN and CMDL sites, though random errors are comparable. Averaging of all-sky LW fluxes over 60-min intervals had little or no effect on the error statistics for the above comparisons. All-sky LW fluxes in these comparisons were, therefore, used at their original temporal resolution (1 or 2 min). This is a result of the fact that the sensitivity of surface LW fluxes to cloud variability is much lower than for SW fluxes.

A small number of points in both Figs. 3a and 3b indicate a significant underestimation of DLFs by the satellite algorithm. Figures 4a and 4b show scatterplots for clear-sky points (from Fig. 3a) separated between day and night. These figures indicate that many more underestimates occur during the night than during the day. The CERES cloud-mask algorithm is based on both visible and infrared (IR) radiances for the day and only on IR radiance for the night. Evidence suggests that a number of nighttime footprints with low clouds are identified as clear by the IR-only cloud algorithm (P. Minnis 2003, personal communication), which results in an underestimation of satellite-derived surface LW fluxes. While ground-based measurements of cloud amount are not available for most of these sites to fully confirm nighttime cloud contamination, limited confirmation was obtained by making use of the ceilometer data available at the ARM/CF. Of the 118 clear-sky points for the ARM/CF listed in Table 2, two points were determined to be cloud contaminated on the basis of the criterion discussed in the next paragraph. Both of these points occurred during nighttime, and ceilometer data corresponding to both indicated the presence of low clouds over ARM/CF with cloud bases in the 200–300-m range. Note that ARM/CF was the only location for which ceilometer data were available for January–August 1998. Also, efforts are under way to remedy the

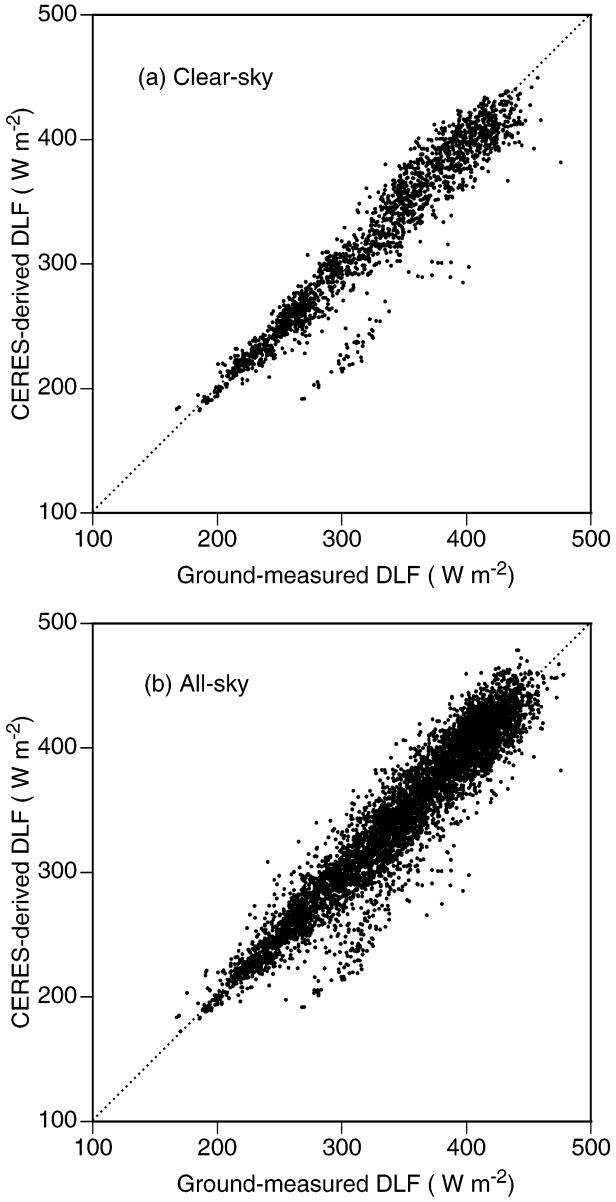

FIG. 3. Comparisons of DLFs derived from the CERES algorithm to ground-based measurements combined for the same sites as in Fig. 2: (a) clear-sky conditions and (b) all-sky conditions. Error statistics for (a) and (b) are presented in the upper and lower boxes of Table 2, respectively. Ground-measured LW fluxes are used at their original 1-min (or 2 min) temporal resolution.

cloud contamination problem by improving nighttime cloud detection in CERES processing.

Separate comparisons for day and night were instrumental in uncovering another source of error in these instantaneous fluxes. The daytime comparison (Fig. 4a) shows that CERES-derived fluxes have a mean bias of about -10 W m^{-2} relative to the ground-measured fluxes. The corresponding mean bias for the nighttime comparison is only about -2 W m^{-2} in spite of a large number of points in this group that show severe underestimation related to cloud contamination. In order to estimate the true magnitude of the nighttime mean bias, an attempt was made to separate the cloud contaminated points from the ones shown in Fig. 4b. A frequency distribution of the DLF difference (CERES derived $-$ ground measured) for these points is shown in Fig. 5 and separates the severely underestimated points from the main distribution at about -50 W m^{-2}. It was assumed that all points in the secondary distribution, that is, with bias lower than -50 W m^{-2} (>50 W m^{-2} in magnitude) were cloud contaminated, and these were screened out of Fig. 4b. The above filter screened out 58 points from the nighttime data. A comparison of the remaining nighttime points is presented in Fig. 4c and shows that the mean bias changed from -1.7 to 2.4 W m^{-2} and there was also a significant reduction in the random error. The results of the above comparisons are presented in Table 3. The same filter, when applied to daytime fluxes, screened out only three points and had a much smaller effect on the mean bias (results not shown).

TABLE 2. Error statistics for comparisons of CERES-derived and ground-measured surface LW fluxes.

Site(s)	No.	Flux (W m^{-2})	Bias (W m^{-2})	RE (W m^{-2})
Clear-sky LW flux statistics				
ARM/CF	118	313.1	-0.8	14.9
ARM/EF	1690	321.2	-4.9	19.5
BSRN	176	298.8	-12.7	14.9
CMDL	61	373.2	-10.6	13.8
All sites	2045	320.3	-5.5	19.0
All-sky LW flux statistics				
ARM/CF	317	339.5	-0.1	18.6
ARM/EF	4470	341.4	-2.5	21.2
BSRN	574	330.5	-9.8	16.0
CMDL	790	380.7	-7.2	16.9
All sites	6151	345.3	-3.7	20.3

Some potential causes were examined for explaining this opposite bias between day and night. One hypothesis considered that the difference might arise from corresponding biases in surface skin temperature present in the operational analysis ECMWF data (MOA) used in CERES processing. Verification of this hypothesis depended on the availability of an independent estimate of the surface skin temperature at the ground sites. Even though direct observations of surface skin temperature at the ground sites were not available, it was possible to derive a proxy dataset from available observations at many sites. Measurements of the upward LW flux from downlooking radiometers mounted on 10-m towers were available for the ARM/CF and all ARM/EF sites and an estimate of surface skin temperature (T_{skin}) for these sites was derived from the measured upward flux, F_u, as

$$T_{\text{skin}} = [\{F_u - (1 - \varepsilon)F_d\}/(\varepsilon\sigma)]^{0.25}, \qquad (4)$$

where F_d is the ground-measured DLF, ε is the surface

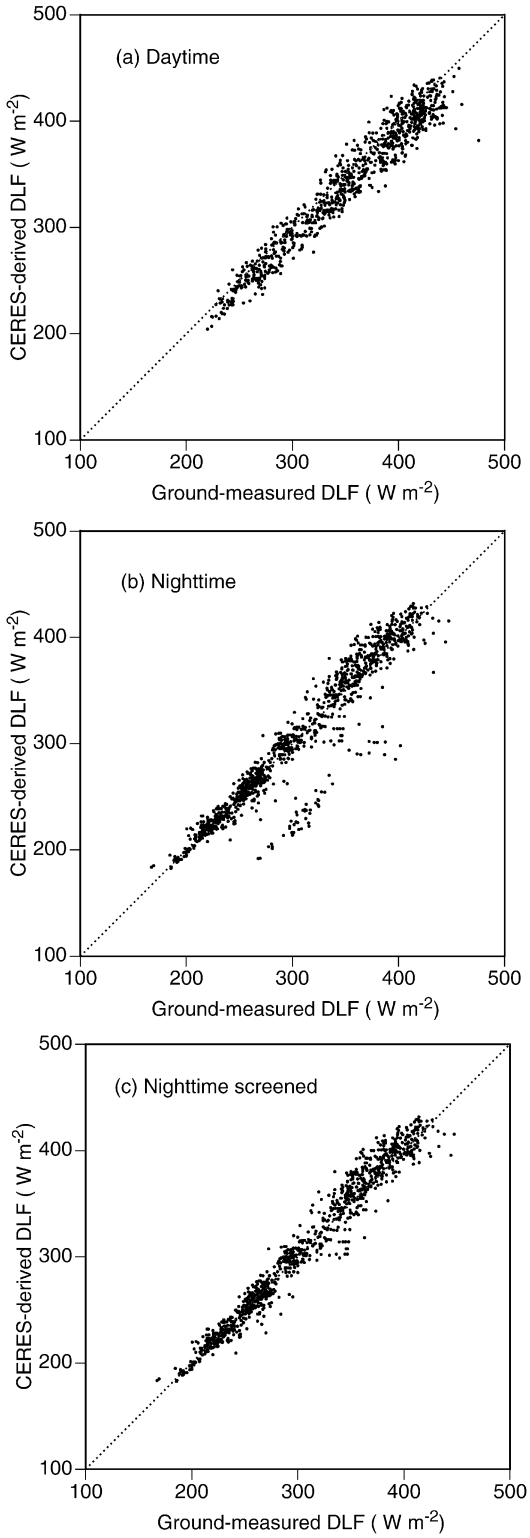

FIG. 4. Comparisons of clear-sky DLFs derived from the CERES algorithm to ground-based measurements (from Fig. 3a) separated between day and night for (a) daytime points, (b) nighttime points, and (c) nighttime points screened for cloud contamination. Error statistics for these comparisons are presented in Table 3. Note that screening of nighttime points for cloud contamination results in a loss of 58 points, a change in the mean bias from −1.7 to 2.4 W m^{-2}, and a significant reduction in the random error.

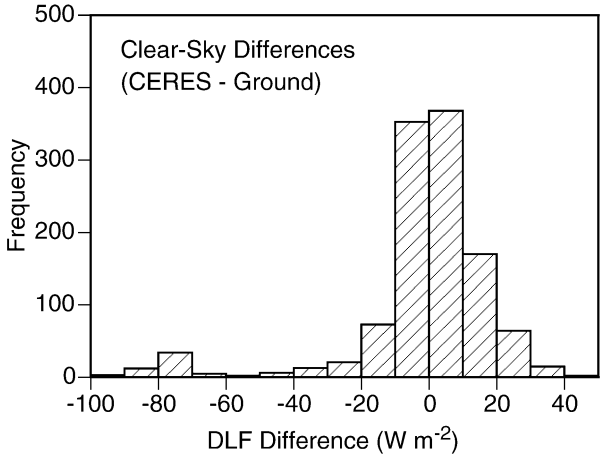

FIG. 5. Frequency distribution of the DLF difference (CERES derived − ground measured) for nighttime clear-sky points from all sites combined. The points in the secondary distribution with biases <-50 W m^{-2} were classified as cloud contaminated.

emissivity [0.99 for ARM/CF and EF sites; Wilber et al. (1999)], and σ is the Stefan–Boltzmann constant. Verification of the above hypothesis was, therefore, limited to the ARM/CF and EF sites. Note that while the area viewed by a downlooking radiometer mounted on a 10-m tower is much smaller than that of a CERES footprint, it may be considered representative of the footprints because the surface type around ARM/SGP sites is fairly uniform cropland.

Figures 6a and 6b show comparisons between surface skin temperature from MOA and that derived from the upward LW flux (ULF) for all clear-sky footprints at ARM/CF and EF, for day and night, respectively. These figures show that, as hypothesized, the average MOA skin temperature is 3.1 K lower for daytime and 1.8 K higher for nighttime compared with the ULF-derived skin temperature. Figures 7a and 7b show, respectively, the comparisons of CERES-derived and ground-measured DLFs for the exact same footprints as are used in Figs. 6a and 6b. The mean values of DLF and T_{skin} shown in Figs. 6 and 7 are presented in Table 4 and show that the opposite day and night biases in CERES-derived DLFs are directly related to corresponding biases in CERES (MOA) T_{skin}. Results in Table 4 also show that the sensitivity of DLF to T_{skin} changes in the two sets are of similar magnitude: 3.3 and 3.1 W m^{-2} K^{-1}, respectively, for CERES-derived and ground-based datasets.

Attempts were also made to examine the potential biases in MOA atmospheric water vapor as a cause of these day–night differences in DLF errors. Microwave radiometer (MWR) measurements of column precipitable wa-

ter (PW) were available from the ARM/CF and a few other sites and were used for this purpose. Comparisons of 1-min averages of MOA and MWR PW values (Figs. 8a and 8b) showed a 3%–4% negative bias (MOA values lower), which did not change much between day and night. Therefore, this PW bias did not contribute to the day–night differences in the DLF errors. This would, however, cause a negative bias of 1.0–1.5 W m^{-2} in the CERES-derived DLF values and may be partly responsible for the DLF biases seen in Table 2.

TABLE 3. Error statistics for comparisons of CERES-derived and ground-measured clear-sky DLFs (combined for all sites) separated between day and night.

Time	No.	Flux (W m^{-2})	Bias (W m^{-2})	RE (W m^{-2})
Daytime	902	341.7	−10.3	14.2
Nighttime	1143	303.4	−1.7	21.4
Nighttime (screened)	1085	306.5	2.4	12.0

5. Summary and conclusions

Validation results are presented for surface SW and LW fluxes derived in CERES processing on an instantaneous–footprint basis. These fluxes, which are a part of the SSF archival product of CERES, were derived using parameterized SW and LW algorithms and meteorological inputs from MOA. The SW and LW algorithms were developed at NASA LaRC and are called the LPSA and LPLA, respectively. The MOA database was derived mainly from ECMWF operational analysis products and is used for all CERES processing. The results presented here are for January–August 1998, during which a CERES instrument successfully operated aboard the *TRMM* satellite. It is noteworthy that the satellite retrievals used in the present comparisons are truly instantaneous. Geostationary satellite retrievals compared in earlier studies (Rossow and Zhang 1995; Gautier and Landsfeld 1997) were 0.5- or 1-h averages. Ground-measured fluxes used for the validation were obtained from ARM/SGP central and extended facilities, and from several sites of the BSRN and CMDL networks. Ground-measured fluxes for all sites were 1-min averages with the exception of one BSRN site (Florianopolis), for which they were 2-min averages. Flux values for all CERES footprints within 10 km of a site were averaged together over 1-min (or 2 min) intervals for comparison with ground-measured fluxes. For all-sky SW comparisons, ground-measured fluxes corresponding to each satellite-derived value were averaged over 60-min intervals to compensate for the spatial variability of clouds within a CERES footprint. Note that even though the solar zenith angle and hence the surface insolation can change considerably over a 60-min interval, they do not contribute large errors to the above comparisons. This is because the instantaneous satellite retrievals are always at the exact midpoint of the 60-min intervals for which the ground-measured fluxes were averaged. A separate comparison of 60-min averages and instantaneous midpoint computations of insolation showed the differences to be 2–5 W m^{-2} (<1% of the mean value), which are much smaller than the scatter present in the all-sky comparisons.

Shortwave errors for both clear-sky and all-sky conditions vary greatly between the groups of sites. Errors for the ARM/CF and EF sites are generally lower than for the BSRN and CMDL sites. Early comparisons for

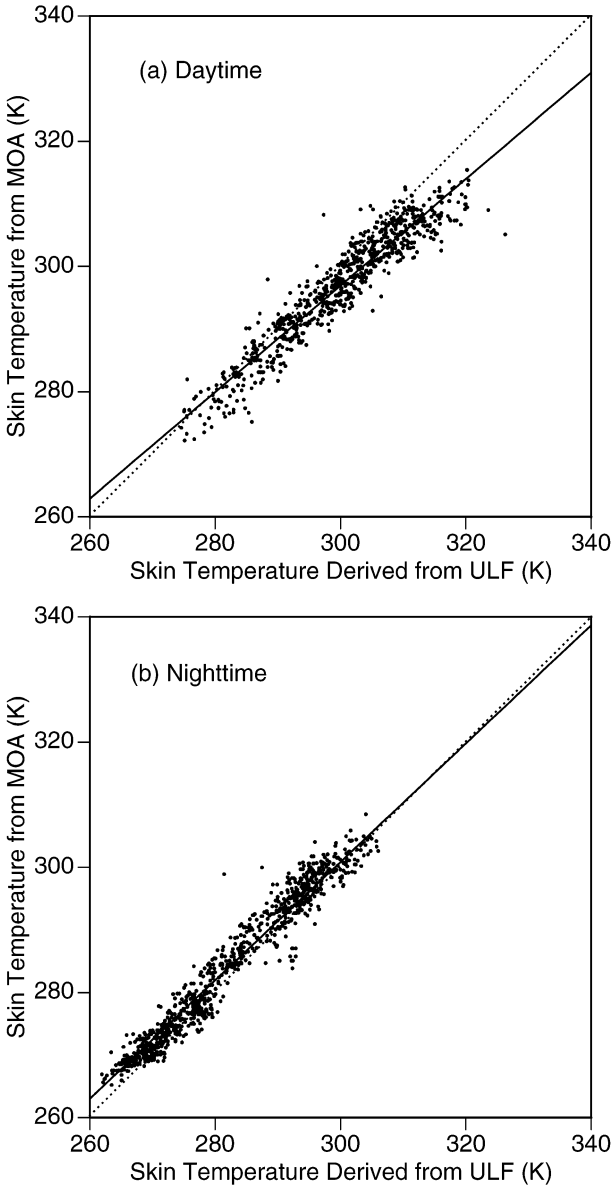

FIG. 6. Comparisons of surface skin temperature from MOA data used by the CERES algorithm to corresponding estimates derived from the upward LW flux at the ARM/CF and ARM/EF sites for clear-sky points: (a) daytime and (b) nighttime points. Note that MOA skin temperatures exhibit a mean bias of −3.1 K for the daytime and 1.8 K for the nighttime. Additional information is presented in the middle box in Table 4.

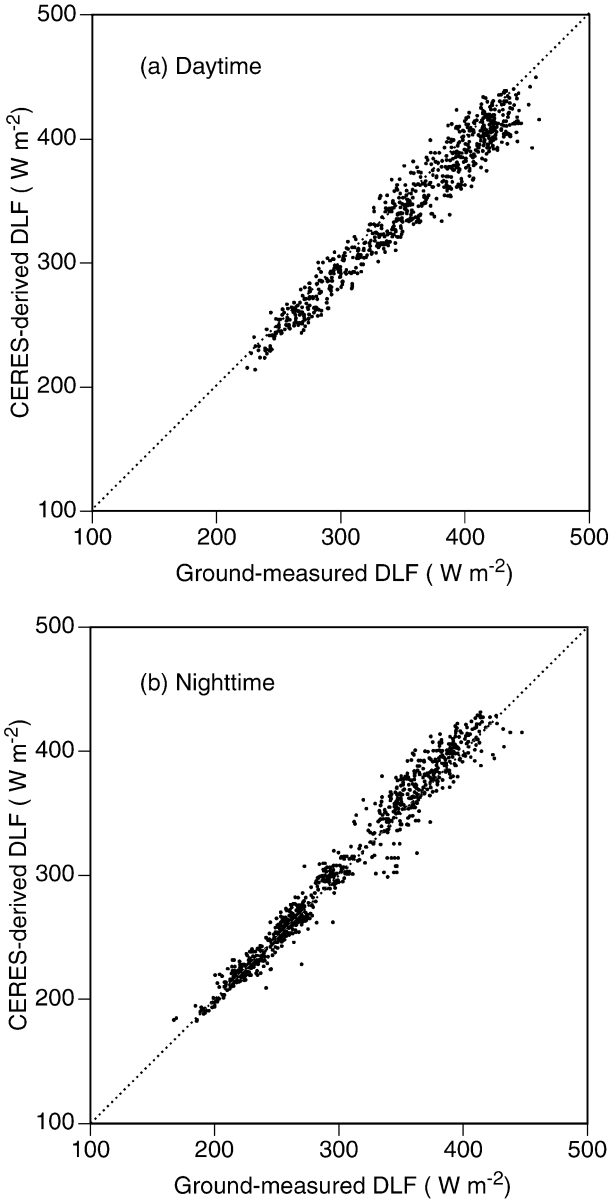

FIG. 7. Comparisons of DLFs derived from the CERES algorithm to ground-based measurements for the same clear-sky points as in Fig. 6: (a) daytime and (b) nighttime points. Note that CERES estimates exhibit a mean bias of −8.9 W m^{-2} for the daytime and 3.4 W m^{-2} for the nighttime, thus establishing a correspondence with the biases in skin temperatures shown in Fig. 6. Additional information is presented in the upper box in Table 4.

some BSRN and CMDL sites showed very large errors and obvious inconsistencies in the site measurements. Once brought to the attention of scientists from the above organizations, such errors were quickly corrected. All biases in the site datasets, known at this time, were corrected for before their use in the comparisons presented here. Random errors for all-sky comparisons were considerably larger than for clear-sky comparisons because of the higher variability associated with clouds.

TABLE 4. Difference between CERES-derived and ground-measured DLFs and corresponding T_{skin}.

	CERES	Ground based
Daytime DLF	345.5	354.4
Nighttime DLF	304.1	300.7
Diff (day–night; in W m^{-2})	41.4	53.7
Daytime T_{skin}	297.1	300.5
Nighttime T_{skin}	284.6	282.8
Diff (day–night; in K)	12.5	17.4
Sensitivity (in W m^{-2} K^{-1})	3.3	3.1

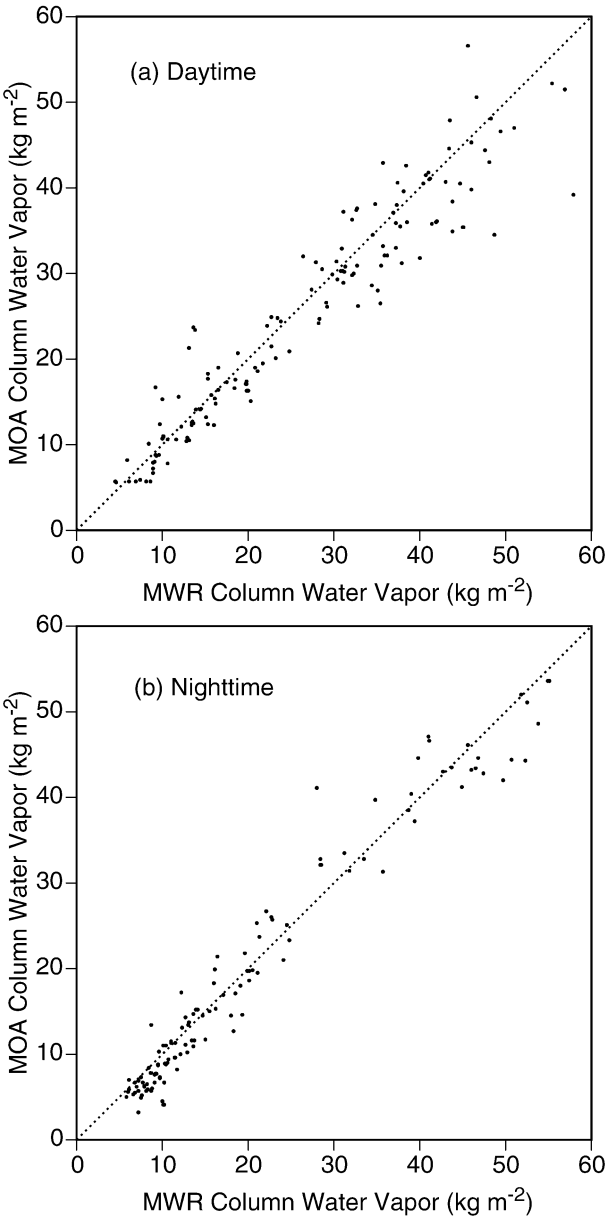

FIG. 8. Comparisons of MOA and MWR column PW for ARM/CF: (a) daytime and (b) nighttime. MOA PW shows a negative bias of 3%–4% for both day and night and does not contribute to the day–night bias differences in DLF.

It should be noted that the larger random errors reported here for SW fluxes do not arise entirely from the satellite retrieval process. They also arise in the surface measurement process and from the small-scale spatial and temporal variability of the insolation fields in the real world (Zelenka et al. 1999). Numerous steps taken in the present work to minimize these effects helped limit the random errors to their present values. Longwave biases and random errors are similar in magnitude for clear-sky and all-sky conditions. Biases for the ARM/SGP sites are lower than for the BSRN and CMDL sites; random errors are comparable.

A small number of points in the clear-sky and all-sky LW comparisons showed significant underestimation of DLF. This is most likely the result of the CERES cloud mask algorithm not being able to detect low clouds, especially at night when the algorithm was based solely on IR radiances. Separation of clear-sky points between day and night did show a preponderance of underestimated points during the night. Limited verification of the above hypothesis was accomplished by using ceilometer data available over ARM/CF. The two clear-sky points from ARM/CF that showed large underestimation of DLF, both occurred during the nighttime and indicated the presence of low clouds with bases in the 200–300-m range. The day–night separation uncovered another source of biases in these instantaneous fluxes. The daytime and nighttime clear-sky points exhibited biases of -10.3 and 2.4 W m^{-2}, respectively. The cause of this day–night bias difference was hypothesized to be the corresponding biases in the surface skin temperature from MOA used in CERES processing. This was verified by comparing MOA skin temperatures with corresponding values derived from upward LW flux measurements available at the ARM/SGP sites. An attempt was also made to examine whether errors in column PW contributed to the above-mentioned day–night differences, by comparing MOA PW with MWR measurements from the ARM/CF site. This comparison showed a 3%–4% negative bias in MOA PW for both day and night. Such a bias would not contribute to the day–night differences but may account for some of the negative bias in DLFs seen in Table 2.

For satellite retrievals of surface radiative fluxes to be useful in climate research, acceptable accuracy requirements are about ± 20 W m^{-2} for instantaneous–footprint values and ± 10 W m^{-2} for monthly gridded products (see Suttles and Ohring 1986). For the instantaneous–footprint SW fluxes presented here, it is clear that at least for some sites there are significant biases, and random errors are much larger than acceptable values. The causes of these errors vary with site and time but generally are in the specification of surface, aerosol, and cloud properties, as well as in the models and the input meteorological data. Errors in the ground-based measurements used for validation are also a contributing factor. Efforts are under way to introduce improved surface albedo maps, aerosol distributions, and cloud radiative properties in the processing. With these changes and better meteorological inputs and ground measurements, the comparisons should improve considerably. For LW comparisons, biases are already lower than for SW, and should be even lower with improved cloud detection at night and better meteorological inputs. Random errors for LW are already close to the acceptable value and should benefit further from the above improvements.

Acknowledgments. The authors are grateful to David Rutan (AS&M) for making the CAVE database available. ARM data are made available through the U.S. Department of Energy as part of the Atmospheric Radiation Measurement program. CMDL data are made available through the NOAA/CMDL Solar and Thermal Radiation (STAR) group. Also, the authors wish to thank the following: (i) the scientists who are responsible for data acquisition at the various BSRN sites, and (ii) B. Wielicki, G. Gibson, and P. Stackhouse (all LaRC) for a critical reading of the manuscript and many valuable suggestions.

REFERENCES

Augustine, J. A., J. J. DeLuisi, and C. N. Long, 2000: SURFRAD—A national surface radiation budget network for atmospheric research. *Bull. Amer. Meteor. Soc.,* **81,** 2341–2357.

Barkstrom, B. R., E. F. Harrison, G. L. Smith, R. N. Green, J. F. Kibler, R. D. Cess, and the ERBE Science Team,1989: Earth Radiation Budget Experiment archival and April 1985 results. *Bull. Amer. Meteor. Soc.,* **70,** 1254–1262.

Charlock, T. P., and Coauthors, 1997: Compute surface and atmospheric fluxes (system 5.0): CERES Algorithm Theoretical Basis Document Release 2.2), NASA/RP-1376, 84 pp. [Available online at http://asd-www.larc.nasa.gov/ATBD/ATBD.html.]

Darnell, W. L., W. F. Staylor, S. K. Gupta, and F. M. Denn, 1988: Estimation of surface insolation using sun-synchronous satellite data. *J. Climate,* **1,** 820–835.

——, ——, ——, N. A. Ritchey, and A. C. Wilber, 1992: Seasonal variation of surface radiation budget derived from ISCCP-C1 data. *J. Geophys. Res.,* **97,** 15 741–15 760.

Ellingson, R. G., J. S. Ellis, and S. B. Fels, 1991: The intercomparison of radiation codes used in climate models: Longwave results. *J. Geophys. Res.,* **96,** 8929–8953.

Gautier, C., and M. Landsfeld, 1997: Surface solar radiation flux and cloud radiative forcing for the Atmospheric Radiation Measurement (ARM) Southern Great Plains (SGP): A satellite, surface observations, and radiative transfer model study. *J. Atmos. Sci.,* **54,** 1289–1307.

Gupta, S. K., 1989: A parameterization for longwave surface radiation from sun-synchronous satellite data. *J. Climate,* **2,** 305–320.

——, W. L. Darnell, and A. C. Wilber, 1992: A parameterization for longwave surface radiation from satellite data: Recent improvements. *J. Appl. Meteor.,* **31,** 1361–1367.

——, A. C. Wilber, W. L. Darnell, and J. T. Suttles, 1993: Longwave surface radiation over the globe from satellite data: An error analysis. *Int. J. Remote Sens.,* **14,** 95–114.

——, ——, N. A. Ritchey, F. G. Rose, T. L. Alberta, T. P. Charlock, and L. H. Coleman, 1997: Regrid humidity and temperature fields (system 12.0). CERES Algorithm Theoretical Basis Document Release 2.2, NASA/RP-1376, 20 pp. [Available online at http://asd-www.larc.nasa.gov/ATBD/ATBD.html.]

——, N. A. Ritchey, A. C. Wilber, C. H. Whitlock, G. G. Gibson, and P. W. Stackhouse Jr., 1999: A climatology of surface radi-

ation budget derived from satellite data. *J. Climate,* **12,** 2691–2710.

——, D. P. Kratz, P. W. Stackhouse Jr., and A. C. Wilber, 2001: The Langley Parameterized Shortwave Algorithm (LPSA) for surface radiation budget studies (version 1.0), NASA/TP-2001-211272, 31 pp. [Available online at http://techreports.larc.nasa.gov/ltrs/ltrs.html.]

Inamdar, A. K., and V. Ramanathan, 1997: On monitoring the atmospheric greenhouse effect from space. *Tellus,* **49B,** 216–230.

Li, Z., H. G. Leighton, and R. D. Cess, 1993: Surface net solar radiation estimated from satellite measurements: Comparisons with tower observations. *J. Climate,* **6,** 1764–1772.

Michalsky, J., E. Dutton, M. Rubes, D. Nelson, T. Stoffel, M. Wesley, M. Splitt, and J. DeLuisi, 1999: Optimal measurement of surface shortwave irradiance using current instrumentation. *J. Atmos. Oceanic Technol.,* **16,** 55–69.

Minnis, P., and Coauthors, 1997: Cloud optical property retrieval (system 4.3). CERES Algorithm Theoretical Basis Document (Release 2.2), NASA/RP-1376, 60 pp. [Available online at http://asd-www.larc.nasa.gov/ATBD/ATBD.html.]

Möser, W., and E. Raschke, 1984: Incident solar radiation over Europe estimated from METEOSAT data. *J. Climate Appl. Meteor.,* **23,** 166–170.

Ohmura, A., and Coauthors, 1988: Baseline Surface Radiation Network (BSRN/WCRP): New precision radiometry for climate change research. *Bull. Amer. Meteor. Soc.,* **79,** 2115–2136.

Peixoto, J. P., and A. H. Oort, 1993: *Physics of Climate.* American Institute of Physics, 520 pp.

Philipona, R., 2002: Underestimation of solar global and diffuse radiation measured at Earth's surface. *J. Geophys. Res.,* **107** (D22), 4654, doi:10.1029/2002JD002396.

Ramanathan, V., 1986: Scientific use of surface radiation budget for climate studies. *Surface Radiation Budget for Climate Applications,* J. T. Suttles and G. Ohring, Eds., NASA RP-1169, 58–86.

Rossow, W. B., and R. A. Schiffer, 1991: ISCCP cloud data products. *Bull. Amer. Meteor. Soc.,* **72,** 2–20.

——, and Y.-C. Zhang, 1995: Calculation of surface and top of atmosphere radiative fluxes from physical quantities based on ISCCP data sets 2. Validation and first results. *J. Geophys. Res.,* **100,** 1167–1197.

Rutan, D. A., F. G. Rose, N. M. Smith, and T. P. Charlock, 2001: Validation data set for CERES Surface and Atmospheric Radiation Budget (SARB). *WCRP/GEWEX News,* Vol. 11, No. 1, International GEWEX Project Office, Silver Spring, MD, 11–12. [Available online at http://www.gewex.org/feb01.pdf; data available online at http://www-cave.larc.nasa.gov/cave/.]

Schmetz, J., 1989: Towards a surface radiation climatology: Retrieval of downward irradiance from satellites. *Atmos. Res.,* **23,** 287–321.

Stackhouse, P. W., S. K. Gupta, S. J. Cox, J. C. Mikovitz, and M. Chiacchio, 2002: New results from the NASA/GEWEX surface radiation budget project: Evaluating El Niño effects at different scales. Preprints, *11th Conf. on Atmospheric Radiation,* Ogden, UT, Amer. Meteor. Soc., 199–202.

Stokes, G. M., and S. E. Schwartz, 1994: The Atmospheric Radiation Measurement (ARM) program: Programmatic background and design of the cloud and radiation testbed. *Bull. Amer. Meteor. Soc.,* **75,** 1201–1221.

Suttles, J. T., and G. Ohring, 1986: Surface radiation budget for climate applications. NASA Ref. Publ. 1169, 132 pp.

Wielicki, B. A., B. R. Barkstrom, E. F. Harrison, R. B. Lee III, G. L. Smith, and J. E. Cooper, 1996: Clouds and the Earth's Radiant Energy System (CERES): An Earth Observing System experiment. *Bull. Amer. Meteor. Soc.,* **77,** 853–868.

Wilber, A. C., D. P. Kratz, and S. K. Gupta, 1999: Surface emissivity maps for use in satellite retrievals of longwave radiation. NASA/TP-1999-209362, 35 pp. [Available online at http://techreports.larc.nasa.gov/ltrs/ltrs.html.]

Wild, M., A. Ohmura, H. Gilgen, and E. Roeckner, 1995: Validation of general circulation model radiative fluxes using surface observations. *J. Climate,* **8,** 1309–1324.

Zelenka, A., R. Perez, R. Seals, and D. Renne, 1999: Effective accuracy of satellite-derived hourly irradiances. *Theor. Appl. Climatol.,* **62,** 199–207.